

# Effect of synthesis conditions on the structural and catalytic properties of hierarchically structured ZSM-5 zeolites

Cite this: *RSC Adv.*, 2014, 4, 13831

Baoyu Liu, Liming Zheng, Zhihong Zhu, Kai Zhang, Hongxia Xi\* and Yu Qian

Hierarchically structured ZSM-5 zeolites were synthesized by employing only one dual-porogenic surfactant, and the hydrothermal crystallization of hierarchical structured zeolites were investigated under rotating and static synthesis conditions. X-Ray diffraction (XRD), Fourier-transform infrared spectroscopy (FTIR), scanning electron microscopy (SEM), transmission electron microscopy (TEM), N<sub>2</sub> adsorption–desorption isotherms, <sup>27</sup>Al magic-angle spinning nuclear magnetic resonance (<sup>27</sup>Al MAS NMR) and thermogravimetric analysis (TGA) were used to characterize the structural and textural features of the resultant zeolite products. By tuning the synthesis conditions from rotating to static, the morphology of the as-obtained hierarchical structure ZSM-5 zeolites changed from silk-like to nanoparticles with a disordered arrangement. Furthermore, the obtained zeolites under static conditions showed a higher BET surface area and lower total pore volume than those of zeolites synthesized under rotating conditions. In addition, quantum chemical calculation results show that the inner ammonium groups may have greater contribution in directing the zeolite structure than tailed ammonium groups. More importantly, the hierarchical structured ZSM-5 zeolites synthesized under static conditions exhibited a higher benzyl alcohol conversion rate and lower ester selectivity compared to those of the samples prepared under rotating conditions. Consideration of the effects of synthesis conditions may be useful for modulating the textural and catalytic properties of hierarchical zeolites.

Received 7th January 2014  
Accepted 3rd March 2014

DOI: 10.1039/c4ra00124a

[www.rsc.org/advances](http://www.rsc.org/advances)

## 1. Introduction

Zeolites are a family of crystalline aluminosilicate materials with a regular arrangement of uniform micropores and have shown great (or potential) applications in many modern industrial processes related to catalysis, adsorption, and separation, especially in the field of petrochemical industry due to the fact that these materials possess high surface area, adjustable pore size, and high thermal and chemical stability.<sup>1,2</sup> So far, 200 structure types of zeolite have been crystallographically classified. Conventional zeolite crystals are normally labeled as ‘molecular sieves’ based on their small pore sizes. This ‘molecular sieving’ effect has enabled the development of molecular size- or shape-selective applications. However, the sole presence of so many micropores often imposes diffusion limitations. Bulky molecules with sizes beyond the micropore dimensions are excluded from the internal zeolite surface. Moreover, even if the smaller molecules could enter the zeolitic micropores, the catalytic performance can be seriously limited by the diffusion of reactants or products in the microporous domains.<sup>3–5</sup> Slow mass transport to and away from the activated

sites can increase the possibility of secondary reactions, which can cause polymerization of by-products or reaction intermediates and result in the formation of cokes.<sup>6</sup> Coke can cover active sites within the microporous channels and leads to catalyst deactivation, decreasing catalytic lifetime in industrial applications.

To resolve the diffusive limitations, mesoporous silica and aluminosilicate materials with larger adjustable pore sizes, such as MCM-41<sup>7</sup> and SBA-15<sup>8</sup> were successively developed in the 1990s. These materials have the ability to overcome the pore size constraints of microporous zeolites and allow the diffusion of larger molecules. Unfortunately, these ordered mesoporous materials show low hydrothermal stability and acidity compared to zeolites crystals, which can be attributed to the fact that the mesopore walls in ordinary mesoporous silica are built with amorphous frameworks. The amorphous nature is a critical factor that prevents their framework acidity from rising to a level that would satisfy use in practical applications, especially in the petrochemical processes. Thus, it is highly desirable to fabricate a hierarchically structured zeolites that possess an open mesoporous structure in addition to microporosity inherent in zeolites. This material can integrate the merits of mesopores and the microporous crystalline structure of zeolites. Mesopores in such crystalline materials are suitable for catalyzing reactions of bulky molecular species that cannot

School of Chemistry and Chemical Engineering, South China University of Technology, Guangzhou, Guangdong 510640, P.R. China. E-mail: [cehxxi@scut.edu.cn](mailto:cehxxi@scut.edu.cn); Fax: +86 020 87113735; Tel: +86 020 87113501

diffuse into the microporous region, while the micropores could provide a size- or shape-selective catalytic process for guest molecules. The hierarchically mesoporous-microporous structure enables zeolites to have maximum structural functions in a limited space.<sup>9</sup>

In the past few decades, there were numerous reports focusing on synthesizing mesoporous aluminosilicate materials with zeolite-like frameworks.<sup>10–17</sup> Among them, typically included are the alkaline or acid leaching of bulk zeolite to generate intracrystalline mesopores,<sup>18–22</sup> fabrication of zeolites in the form of small nanoparticles in order to form mesoporous channels by intercrystalline void space,<sup>14</sup> adding the ‘hard’ templates as a mesopore structure-directing-agent (SDA) to prepare zeolites containing mesopores,<sup>23–25</sup> and incorporating the ‘soft’ templates into the zeolite framework as a mesopore-generating agent to synthesize the mesoporous zeolites.<sup>15,26,27</sup>

In this respect, a great breakthrough has been made by Ryoo's research group.<sup>28,29</sup> A series of gemini-type multi-ammonium surfactants were used as structure directing agents for hierarchically structured zeolites with crystalline microporous frameworks.<sup>30–33</sup> These surfactants are composed of hydrophilic quaternary ammonium groups and hydrophobic alkyl chain moieties. The ammonium head groups caused the silica precursor to form the microporous crystalline zeolitic framework while the self-assembled surfactant tails directed the zeolite crystal morphology into a mesostructure. These surfactants played a dual structure-directing functional role as both a zeolite-structure-directing agent and mesoporosity-generating template in the absence of other SDAs. It is quite attractive to fabricate hierarchical zeolites using such a dual-functional surfactant approach.

Herein, extending their work, we report the results obtained by employing a bifunctional tetra-quaternary ammonium type surfactant as SDA to synthesize hierarchically structured ZSM-5 zeolites under static and rotating conditions. This study was undertaken to investigate the effect of synthesis conditions for zeolite structure generation. The zeolite structure, porosity, morphology and catalytic performance were analyzed by complementary combination of X-ray diffraction, N<sub>2</sub> adsorption, electron microscopy and probe reaction. Besides, we study the molecular properties of the surfactant by means of the density functional theory (DFT) method. We report these results because this information may provide valuable guidance for practical industrial applications.

## 2. Experimental

### 2.1. Synthesis of organic surfactant

The tetra-quaternary ammonium surfactant is synthesized according to the literature procedures.<sup>29</sup> In a typical synthesis, first 0.01 mol of 1-bromodocosane (98%, J&K) and 0.1 mol of *N,N,N',N'*-tetramethyl-1,6-hexanediamine (99%, J&K) were dissolved in 50 mL toluene-acetonitrile mixture with *v/v* = 1 : 1, then the mixture was refluxed with stirring for 8 h at 65 °C, after cooling to room temperature and solvent evaporation, the precipitated product was [C<sub>22</sub>H<sub>45</sub>-N<sup>+</sup>(CH<sub>3</sub>)<sub>2</sub>-C<sub>6</sub>H<sub>12</sub>-N(CH<sub>3</sub>)<sub>2</sub>]<sup>+</sup>[Br<sup>-</sup>]. The precipitate was collected by filtration and washed

with diethyl ether, and dried in a vacuum oven at 50 °C for 8 h. Second, 0.005 mol of the [C<sub>22</sub>H<sub>45</sub>-N<sup>+</sup>(CH<sub>3</sub>)<sub>2</sub>-C<sub>6</sub>H<sub>12</sub>-N(CH<sub>3</sub>)<sub>2</sub>]<sup>+</sup>[Br<sup>-</sup>] and 0.0025 mol 1,6-dibromohexane (98%, J&K) were dissolved in 40 mL of acetonitrile, then the mixture was refluxed with stirring for 12 h at 75 °C, after cooling to room temperature and solvent evaporation, the precipitated product was collected by filtration and washed with diethyl ether, and dried in a vacuum oven at 50 °C for 8 h to obtain the final product, the [C<sub>22</sub>H<sub>45</sub>-N<sup>+</sup>(CH<sub>3</sub>)<sub>2</sub>-C<sub>6</sub>H<sub>12</sub>-N<sup>+</sup>(CH<sub>3</sub>)<sub>2</sub>-C<sub>6</sub>H<sub>12</sub>-N<sup>+</sup>(CH<sub>3</sub>)<sub>2</sub>-C<sub>6</sub>H<sub>12</sub>-N<sup>+</sup>(CH<sub>3</sub>)<sub>2</sub>-C<sub>22</sub>H<sub>45</sub>]<sup>4+</sup>[Br<sup>-</sup>]<sub>4</sub> surfactant, which is hereby designated as C<sub>22</sub>-N<sub>4</sub>-C<sub>22</sub>. The purity of the final solid product was analyzed by <sup>1</sup>H-NMR measurements in a CD<sub>3</sub>OD solution with a Bruker Avance Digital 400 spectrometer.

### 2.2. Synthesis of the hierarchically structured ZSM-5 zeolites

In a typical synthesis, a homogeneously mixed solution was first prepared from fumed Silica (99%, J&K), C<sub>22</sub>-N<sub>4</sub>-C<sub>22</sub> surfactant, NaAlO<sub>2</sub> (44.7 wt% Na<sub>2</sub>O, 52 wt% Al<sub>2</sub>O<sub>3</sub>, J&K), NaOH, ethanol and H<sub>2</sub>O with a molar ratio of 5.43Na<sub>2</sub>O–24SiO<sub>2</sub>–0.6Al<sub>2</sub>O<sub>3</sub>–1.2C<sub>22</sub>-N<sub>4</sub>-C<sub>22</sub>–192ethanol–1706H<sub>2</sub>O. The resultant gel mixture was aged under magnetic stirring at 65 °C for 12 h. The final gel obtained was transferred into 50 mL Teflon-lined stainless steel autoclave and heated at 150 °C under rotating and static conditions for 5 days respectively. After crystallization, the products were collected by filtration, dried in air, and calcined at 580 °C for 6 h to remove the template. The resulting hierarchically structured ZSM-5 zeolites samples are denoted by ZSM-5-R (rotating) and ZSM-5-S (static) respectively. For comparison, a conventional ZSM-5 sample was purchased from Nankai University catalyst Co., Ltd, which is denoted by ZSM-5-C.

### 2.3. Characterization

Powder X-ray diffraction (XRD) patterns were recorded on a Rigaku Rotaflex Diffractometer using CuKα radiation ( $\lambda = 1.5418 \text{ \AA}$ ). N<sub>2</sub> adsorption-desorption isotherms were measured with a Micromeritics ASAP 2020 system at 77 K. The samples were outgassed for 12 h at 150 °C before the measurements. The specific surface areas of the materials were calculated from the adsorption branch of the isotherm using the Brunauer-Emmett-Teller (BET) equation, and the pore-size distribution was analyzed by using the Barrett-Joyner-Halenda (BJH) method. Scanning Electron Microscopy (SEM) images were recorded with a Carl Zeiss, ZEISS Ultra 55 at a low landing energy (5.0 kV). Samples were mounted using a conductive carbon double-sided sticky belt, and a thin coating of gold sputter was deposited onto the samples in order to reduce the effects of charging. Transmission Electron Microscopy (TEM) images were recorded with a JEOL JEM-2100 electron microscope operated at 200 kV and equipped with a Gatan 832 CCD camera. The FTIR spectra of samples in the form of KBr pellets were recorded at room temperature on a Bruker Vector 33-IR spectrometer with a resolution of 1 cm<sup>-1</sup>. The thermal behaviour of a washed, as-synthesized sample was observed on a Perkin Elmer Pyris 6 TGA analyzer with a heating rate of 5 °C min<sup>-1</sup> under a nitrogen flow of 30 mL min<sup>-1</sup>. <sup>27</sup>Al MAS NMR spectra were recorded on a Bruker Avance AV 400 spectrometer

at 104.26 MHz. A saturated aqueous aluminium sulfate solution with a chemical shift 0.0 ppm was used as an external reference.

## 2.4. Calculations

DFT methods have become very popular recently due to accuracies that are similar to other methods while requiring less time and smaller investments from a computational point of view.<sup>34</sup> In this work, a hybrid functional B3LYP level at the 6-31G\* basis set was adopted to calculate molecular structure and electronic density of the cationic C<sub>22</sub>-N<sub>4</sub>-C<sub>22</sub> surfactant. This basis set provided accurate geometry and electronic properties for a wide range of organic compounds.<sup>35,36</sup> All the calculations were performed using the Gaussian 03 program package. Besides, molecular electrostatic potential (MEP) and frontier molecular orbitals were determined at the same level of theory B3LYP/6-31G\* with the optimized structure.

## 2.5. Catalytic reaction

Before the catalytic tests, all the samples were ion-exchanged three times with 1 M NH<sub>4</sub>NO<sub>3</sub> solution at 90 °C and then converted to the H<sup>+</sup> form *via* calcination in flowing nitrogen (120 mL min<sup>-1</sup>) at 550 °C for 6 h. Here, the esterification reaction of benzyl alcohol and hexanoic acid was chosen as a model reaction involving large molecules in order to compare the catalytic ability of ZSM-5-R, ZSM-5-S and ZSM-5-C. In a typical reaction, a reaction mixture containing toluene (12 mL), benzyl alcohol (15 mmol), hexanoic acid (18 mmol) and catalyst (0.2 g) was heated under stirring at 110 °C for 6 h in a three-necked flask with a reflux condenser under N<sub>2</sub> atmosphere. After the reaction, the mixture was centrifuged and analyzed using a GC-MS (QP2010) and Waters HPLC system (UV detection wavelength was set at 257 nm).

# 3. Results and discussion

## 3.1. Characterization of the hierarchically structured ZSM-5 zeolites

The X-ray diffraction patterns of hierarchical structure ZSM-5 zeolite samples synthesized under rotating and static

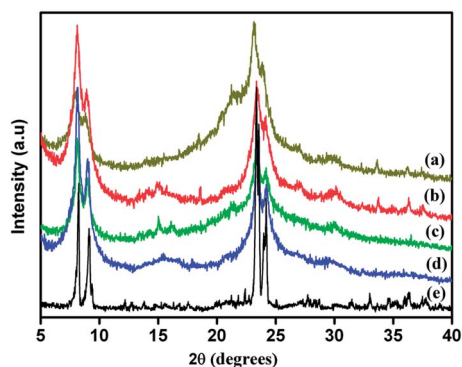


Fig. 1 Wide-angle XRD patterns of (a) as-synthesized ZSM-5-R, (b) calcined ZSM-5-R at 580 °C, (c) as-synthesized ZSM-5-S, (d) calcined ZSM-5-S at 580 °C and (e) conventional ZSM-5.

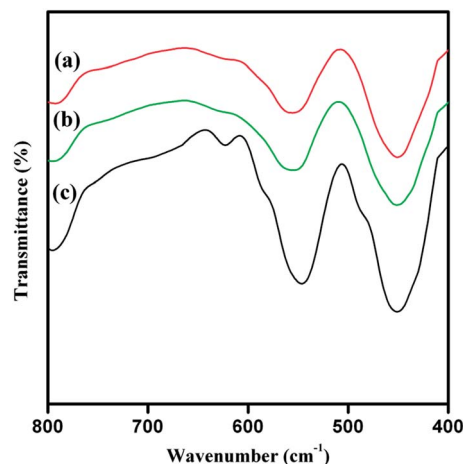


Fig. 2 IR spectra of samples: (a) ZSM-5-R, (b) ZSM-5-S and (c) ZSM-5-C.

conditions are shown in Fig. 1. The XRD patterns confirm that all samples are highly crystallized ZSM-5 zeolite, exhibiting the characteristics of a crystalline MFI reported by Ryoo *et al.*<sup>29</sup> Comparing the as-synthesized and calcined ZSM-5-R with ZSM-5-S samples reveals that the diffraction patterns of ZSM-5-R have a more broader peaks than those of ZSM-5-S samples respectively. However, the XRD patterns of ZSM-5-R and ZSM-5-S samples are well matched to reflections of ZSM-5-C sample, and no other crystalline phase was detected. In addition, upon removal of the surfactant by calcinations at high temperature, the intensity of Bragg reflection of the calcined ZSM-5-R and ZSM-5-S increases to some extent compared with the as-synthesized ZSM-5-R and ZSM-5-S respectively, suggesting that the calcination process may promote siloxane cross-linking and thereby somewhat improve the ordering of the framework.<sup>37</sup>

The FT-IR test was carried out to further identify the crystal phase (Fig. 2), all of the samples show a broad band at 451 cm<sup>-1</sup> in the region of 400–500 cm<sup>-1</sup>, which corresponds to a Si–O bending mode observed in all amorphous SiO<sub>2</sub> materials.<sup>38</sup> However, other another absorptions at 545, 553 and 551 cm<sup>-1</sup> were detected in the spectrum of ZSM-5-C, ZSM-5-R and ZSM-5-S respectively, which can be generally attributed to the five-membered rings of T–O–T (T = Si or Al) in MFI-type zeolites,<sup>39</sup> indicating that the ZSM-5-R/ZSM-5-S samples contain the primary units of zeolite MFI. In addition, a band is observed at about 622 cm<sup>-1</sup> only in the ZSM-5-C sample, which is evidence for a higher extent of zeolitisation.<sup>40</sup>

Fig. 3 shows the SEM and TEM images of ZSM-5-R and ZSM-5-S samples. The ZSM-5-S sample, shown in Fig. 3a, is comprised of nanoparticles with a randomly organized structure, while ZSM-5-R sample exhibits a silk-like morphology (Fig. 3b). No physically isolated crystals or particles of the two phases were detected throughout the entire ZSM-5-R/ZSM-5-S samples. SEM only shows the surface morphology of the hierarchically structured ZSM-5 zeolites. A close examination on each sample was conducted by TEM observation (results shown in Fig. 3c–f). Fig. 3c shows the TEM image of ZSM-5-R, which exhibits aggregation of short piece-like morphology, and these individual short pieces were assembled irregularly.

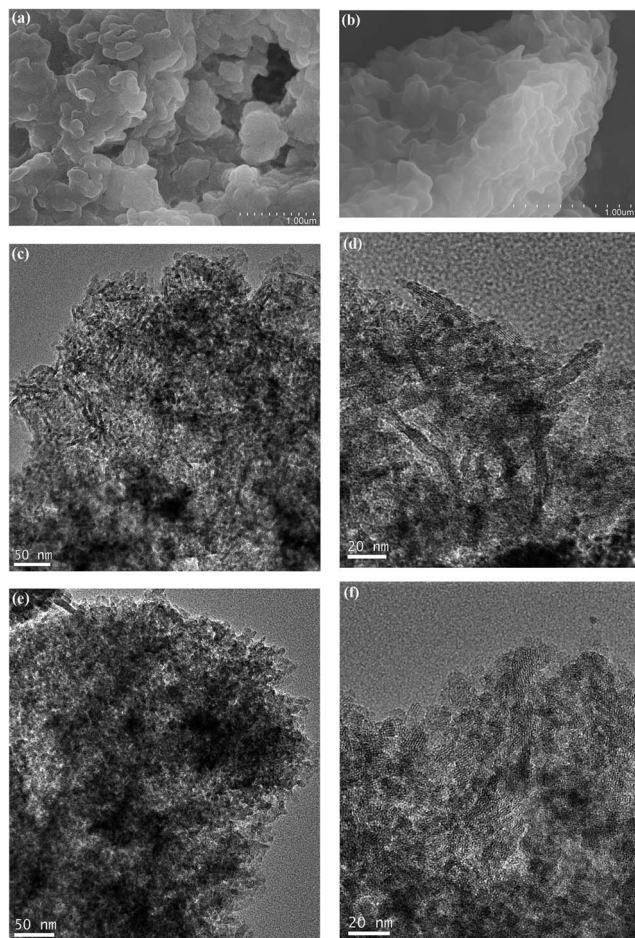


Fig. 3 SEM images of as-synthesized products: (a) ZSM-5-S and (b) ZSM-5-R; TEM images of as-synthesized samples: (c) and (d) for ZSM-5-R, (e) and (f) for ZSM-5-S at different magnifications.

Furthermore, the lattice fringe can be clearly seen in the high-resolution TEM (HR-TEM) image of the ZSM-5-R sample (Fig. 3d). ZSM-5-S sample shown in Fig. 3e and f, however, indicates a fully crystalline structure with mesopores penetrating through the micropore nanoparticle frameworks. Amorphous silica domains were not detected in electron microscopic images for either of the ZSM-5-R and ZSM-5-S samples. These results indicated that the morphology of final samples can be affected through rotating and static synthesis conditions.

$N_2$  adsorption-desorption isotherms were used to reveal the porosity features of parents ZSM-5-R and ZSM-5-S samples. Fig. 4 shows that the synthesized ZSM-5-R and ZSM-5-S samples exhibit type-IV  $N_2$  isotherms with a hysteresis loop corresponding to capillary condensation at high relative pressure, suggesting a relatively large mesopore size. Comparatively, no obvious  $N_2$  condensation can be observed at  $P/P_0 > 0.1$  for ZSM-5-C zeolite, indicating a traditional microporous material without mesopores. At relatively low pressures ( $P/P_0 < 0.02$  corresponding to the micropore filling), all the samples have similar isotherms, indicating that they have similar microporous structures. In the higher relative pressure region ( $P/P_0 >$

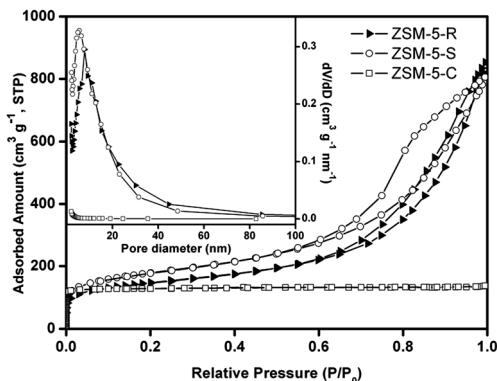


Fig. 4 Nitrogen adsorption-desorption isotherms and pore size distributions of ZSM-5-S, ZSM-5-R and ZSM-5-C.

0.6), the ZSM-5-R and ZSM-5-S samples show different hysteresis loops, indicating they have different mesoporous and/or macroporous structures. For the ZSM-5-R samples, the hysteresis loop has the general type A form, indicating that the ZSM-5-R samples have well-defined cylindrical-like pore channels.<sup>41</sup> For the ZSM-5-S samples, the hysteresis loop shows the general type B form, which shows that the material has slit-shaped pores, and the distribution of pore size and/or shape is not well defined.<sup>41</sup> Correspondingly, the Barrett-Joyner-Halenda (BJH) model was used to estimate the mesopore size distributions of ZSM-5-R, ZSM-5-S and ZSM-5-C samples. The results exhibit mesopores in the range of 2.3–31 nm, centered at 7.5 and 5.6 nm for ZSM-5-R and ZSM-5-S respectively. In contrast, the ZSM-5-C sample does not contain any mesopores. A more detailed analysis (Table 1) reveals that the ZSM-5-S samples have higher BET surface areas and external surface areas compared with ZSM-5-R samples. However, the total pore volumes and microporous volumes of ZSM-5-S are smaller than those of ZSM-5-R. These different textural properties of the ZSM-5-R and ZSM-5-S samples may be due to the different synthesis conditions of the zeolites.

$^{27}\text{Al}$  MAS NMR technique is a well-established tool to determine the coordinations of the aluminum species present in the zeolite samples,<sup>42</sup> and the chemical activity of aluminosilicate materials is generally correlated to the presence of intra-framework aluminium atoms incorporated into the silica framework.<sup>43</sup> The coordination state of Al in the ZSM-5-R and ZSM-5-S was checked by  $^{27}\text{Al}$  MAS NMR spectroscopy (Fig. 5). It is clear that both ZSM-5-R and ZSM-5-S exhibit a single resonance peak at a chemical shift of 60.22 and 60.13 respectively, which can be assigned to the Al species with a tetrahedrally coordinated framework. Compared with the tetrahedral Al signal, the absence of a peak at 0 ppm in both ZSM-5-R and ZSM-5-S samples suggests that there is no non-framework octahedrally coordinated Al, which demonstrates that Al is entirely incorporated in the framework of the sample. However, in the ZSM-5-R sample, the NMR peak corresponding to the intra-framework Al was slightly broad compared with that of ZSM-5-S sample, which could be attributed to the different conditions employed during zeolite synthesis, resulting in slight differences in the environments around Al in the zeolite frameworks.

Table 1 Textual properties of the selected samples

Sample	Si/Al <sup>a</sup>	$S_{\text{BET}}^b$ [m <sup>2</sup> g <sup>-1</sup> ]	$S_{\text{ext}}^c$ [m <sup>2</sup> g <sup>-1</sup> ]	$S_{\text{mic}}^c$ [m <sup>2</sup> g <sup>-1</sup> ]	$V_{\text{tot}}^c$ [cm <sup>3</sup> g <sup>-1</sup> ]	$V_{\text{ext}}^d$ [cm <sup>3</sup> g <sup>-1</sup> ]	$V_{\text{mic}}^c$ [cm <sup>3</sup> g <sup>-1</sup> ]
ZSM-5-C	20	347	132	215	0.25	0.09	0.16
ZSM-5-S	17	630	439	191	1.18	1.03	0.15
ZSM-5-R	19	518	355	163	1.32	1.19	0.13

<sup>a</sup> Si/Al ratio was obtained by ICP/AES analysis. <sup>b</sup>  $S_{\text{BET}}$  is the specific BET surface area obtained from N<sub>2</sub> adsorption. <sup>c</sup> Micropore and external surface areas and micropore volumes by *t*-plot method. <sup>d</sup> Total pore volumes is obtained at  $P/P_0 = 0.95$ .

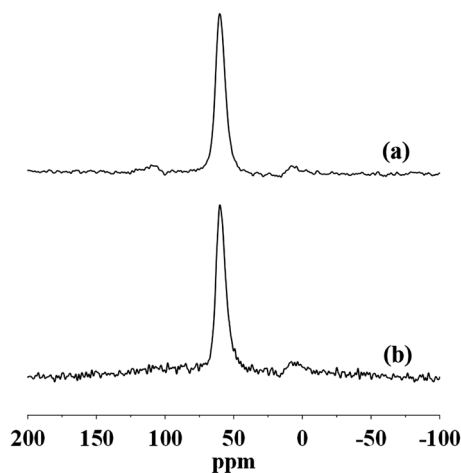
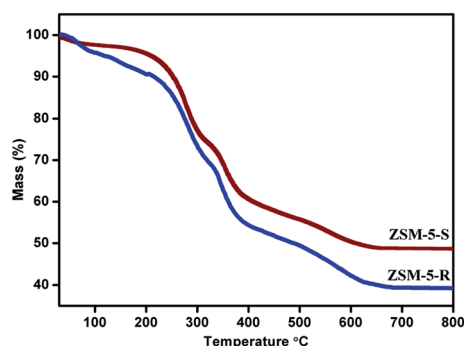
Fig. 5 <sup>27</sup>Al MAS NMR spectra of (a) ZSM-5-R and (b) ZSM-5-S.

Fig. 6 Thermogravimetric (TG) curves of as-synthesized ZSM-5-R and ZSM-5-S.

Thermogravimetric analysis (TGA) of the as-synthesized ZSM-5-R and ZSM-5-S samples using the C<sub>22</sub>-N<sub>4</sub>-C<sub>22</sub> template in the presence of nitrogen is presented in Fig. 6. Both the ZSM-5-R and ZSM-5-S exhibit four distinct regions of weight loss. The first weight loss below 140 °C is attributed to desorption of physically adsorbed water in the porous material. Very significant weight losses were recorded with three steps in the temperature ranges of 140–310 °C, 310–400 °C and 400–700 °C respectively, which could be assigned reasonably to the complete cracking and combustion of the surfactant

incorporated in the hierarchical structure. It is important to note that the dual functional surfactant can interact strongly with the zeolite framework, so it is removed in later stages.<sup>16</sup> However, compared with ZSM-5-R, the amount of the weight loss for ZSM-5-S was lower in all temperature ranges. This result indicates that the ZSM-5-R may have a relatively larger pore volume than that of ZSM-5-S, which is consistent with the results of textural analysis using N<sub>2</sub> adsorption.

### 3.2. Computational study

The surfactant used in the present work was composed of four quaternary ammoniums connected with -C<sub>6</sub>H<sub>12</sub>- alkyl spacers and two hydrophobic -C<sub>22</sub>H<sub>45</sub> alkyl tails. Such a cationic amphiphilic surfactant could easily disperse into the synthesis solution and assemble cooperatively with silicate anions to generate hierarchical structure ZSM-5 zeolite, in which the multi-ammonium head group acted as an effective structure-directing agent for the microporous zeolite, while the hydrophobic interaction between the long-chain tails induced the formation of a mesoscale micellar structure. Herein, quantum chemical calculations were performed in order to investigate the molecular structure and electronic density of the cationic C<sub>22</sub>-N<sub>4</sub>-C<sub>22</sub> surfactant. Molecular electrostatic potential (MEP) is related to the electronic density and is a very useful tool in understanding the sites for electrophilic attack and nucleophilic reactions.<sup>44</sup> To predict reactive sites for nucleophilic attack for the title surfactant, MEP was calculated based on optimized geometry (Fig. 7a). MEP image (Fig. 7b) shows that the positive (blue/cyan) regions are mainly over the ammonium groups, especially on the inner ammonium groups when compared to the two tailed ammonium groups [N<sup>+</sup>(CH<sub>3</sub>)<sub>2</sub> bonded directly to the C<sub>22</sub>H<sub>45</sub> tail], indicating that the preferred sites for nucleophilic attack that is relevant to anionic aluminosilicate species are the inner ammonium groups, followed by the tailed ammonium groups.<sup>45</sup>

The frontier orbital of a chemical species is very important in defining its reactivity.<sup>46</sup> Fig. 7c shows the electric/orbital density distributions of LUMO (the lowest unoccupied molecular orbital) for the surfactant. The LUMO represents the ability of the molecule to accept electrons. The lower value of LUMO indicates the molecule accepts electrons more probable. As can be seen from Fig. 7c, the LUMO is located in the inner two ammonium groups, indicating that the inner ammonium groups may have more contribution as the zeolite-structure-directing function than two tailed ammonium groups. A similar

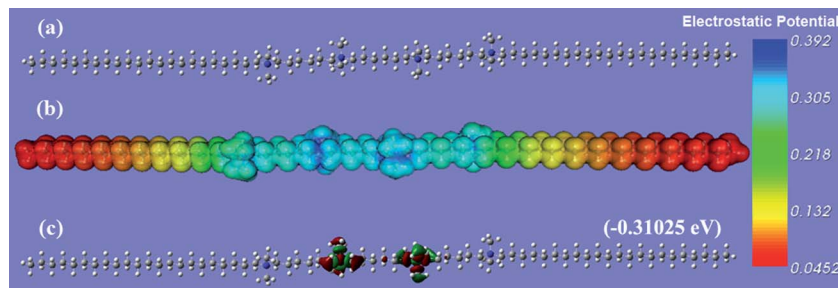


Fig. 7 (a) Optimized structure (b) molecular electrostatic potential map and (c) molecular orbital surface and energy level of the 'bifunctional' cationic surfactant (atom legend: white = H; gray = C; blue = N).

conclusion was drawn by Jung *et al.*<sup>47</sup> and Park *et al.*<sup>30</sup> who confirmed that the gemini-type surfactants containing only the tailed ammoniums were unable to generate any zeolite frameworks at all.

### 3.3. Catalytic activity

The liquid phase esterification reaction of benzyl alcohol and hexanoic acid (Fig. 8) was employed as a probe reaction to examine the catalytic performances of ZSM-5-R and ZSM-5-S in a diffusion-constrained reaction. It can be seen from Fig. 8, compared with ZSM-5-C, ZSM-5-R and ZSM-5-S exhibit higher benzyl alcohol conversions. Because the esterification reaction involves large molecular species, it may take place primarily at the surface of mesopore walls. Thus, the low conversion of ZSM-5-C could be attributed to a diffusion limitations due to its small pore diameter. The high catalytic activities of ZSM-5-R and ZSM-5-S indicate that interconnected micropore-to-mesopore and mesopore-to-mesopore frameworks can lead to easier access to the active sites for reactants and faster diffusion of products during the reaction.

On the other hand, the ZSM-5-S exhibited a higher benzyl alcohol conversion rate of 69% than that of ZSM-5-R (51%). We attribute the difference between ZSM-5-S and ZSM-5-R to their differences in external surfaces and average pore diameters. The

average pore diameter of ZSM-5-S is less than that of ZSM-5-R, indicating that ZSM-5-R has better diffusion property than that of ZSM-5-S. However, the esterification reaction is mainly catalyzed by Brønsted acids located at the surface of the mesopore walls.<sup>48</sup> While ZSM-5-S has higher external surface area than that of ZSM-5-R, which suggests that ZSM-5-S can supply more active sites for the catalytic reaction than those of ZSM-5-R. From this point of view, the external surface area played a decisive factor. Thus, ZSM-5-S exhibited a higher conversion of benzyl alcohol than that of ZSM-5-R. The ester selectivity of ZSM-5-C, ZSM-5-R and ZSM-5-S was 91.4%, 64.9% and 53.6%, respectively. The ZSM-5-C exhibited the highest ester selectivity due to the sole presence of micropores inhibiting the dehydrative condensation between two alcohol molecules.<sup>49</sup> The average pore diameter may be responsible for the difference of ester selectivity between ZSM-5-S and ZSM-5-R. The large average pore diameter could increase the diffusion freedom of moleculars, resulting in low selectivity. Apparently, the hierarchically structured ZSM-5 zeolites exhibit a remarkable benefit for the model esterification reaction of benzyl alcohol and hexanoic acid. Furthermore, the hierarchically structured zeolites can be extended to many other catalytic reactions involving large molecules, where diffusion constraints and/or adsorption of reactant molecules onto the acid sites are the main concern.

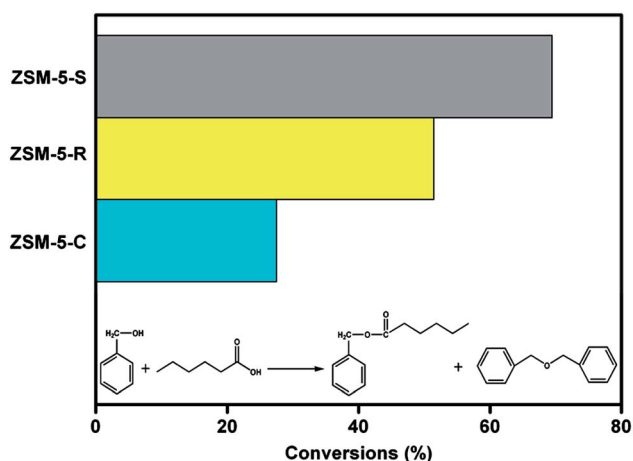


Fig. 8 Catalytic activity of ZSM-5-S, ZSM-5-R and ZSM-5-C in the esterification reaction of benzyl alcohol and hexanoic acid.

## 4. Conclusion

A tetra-quaternary ammonium type surfactant was employed as SDA to synthesize hierarchically structured ZSM-5 zeolites under rotating and static conditions in this study. By tuning the synthesis conditions (rotating and static), the morphology and porosity of the resultant zeolites were changed. The resulted samples exhibited piece-like morphology and nanoparticle frameworks under rotating and static conditions, respectively. Besides that, the ZSM-5-S sample showed higher BET surface areas and external surface areas than those of ZSM-5-R samples. Nevertheless, the total pore volumes and microporous volumes of ZSM-5-S were smaller compared to ZSM-5-R. In addition, quantum chemical calculations were used to gain more information about the molecular structure of the dual-functional tetra-quaternary ammonium type surfactant. Moreover, the hierarchical structure ZSM-5-R and ZSM-S zeolites showed

different catalytic activities in case of esterification reaction of benzyl alcohol and hexanoic acid. The ZSM-5-S exhibited a higher benzyl alcohol conversion rate and lower ester selectivity than those of ZSM-5-R. The present study indicates that the different synthesis conditions (rotating and static) can change the textural and catalytic properties of hierarchical structure ZSM-5 zeolites guided by  $C_{22}-N_4-C_{22}$  templates. Further work would be necessary for a detailed investigation concerning the effects of synthesis conditions on the structural and catalytic properties for targeted catalytic reactions. In a word, the effect of synthesis conditions (rotating and static) provided here would be helpful for investigating the hydrothermal crystallization of other zeolites under various synthesis conditions in the future. Further research is currently under way in our laboratory.

## Acknowledgements

This work was supported by the National Natural Science Foundation of China (no. 20936001 and 21176084), the National High Technology Research and Development Program of China (no. 2013AA065005), SRFDP (no. 20130172110012) and Guangdong Natural Science Foundation (S2011 030001366) are gratefully acknowledged.

## References

- W. F. Höelderich and G. Heitmann, *Catal. Today*, 1997, **38**, 227–233.
- M. J. Verhoef, P. J. Kooyman, J. C. van der Waal, M. S. Rigutto, J. A. Peters and H. van Bekkum, *Chem. Mater.*, 2001, **13**, 683–687.
- P. Matias, J. M. Lopes, S. Laforge, P. Magnoux, M. Guisnet and F. R. Ribeiro, *React. Kinet. Catal. Lett.*, 2008, **95**, 193–201.
- I. Fechete, P. Caultet, E. Dumitriu, V. Hulea and H. Kessler, *Appl. Catal., A*, 2005, **280**, 245–254.
- S. Eriksson, U. Nylén, S. Rojas and M. Boutonnet, *Appl. Catal., A*, 2004, **265**, 207–219.
- R. Srivastava, M. Choi and R. Ryoo, *Chem. Commun.*, 2006, 4489–4491.
- C. T. Kresge, M. E. Leonovicz, W. J. Roth, J. C. Vartuli and J. S. Beck, *Nature*, 1992, **359**, 710–712.
- D. Y. Zhao, J. L. Feng, Q. S. Huo, N. Melosh, G. H. Fredrickson, B. F. Chmelka and G. D. Stucky, *Science*, 1998, **279**, 548–552.
- K. Na, M. Choi and R. Ryoo, *Microporous Mesoporous Mater.*, 2013, **166**, 3–19.
- C. J. H. Jacobsen, C. Madsen, J. Houzvicka, I. Schmidt and A. Carlsson, *J. Am. Chem. Soc.*, 2000, **122**, 7116–7117.
- I. Schmidt, A. Boisen, E. Gustavsson, K. Ståhl, S. Pehrson, S. Dahl, A. Carlsson and C. J. H. Jacobsen, *Chem. Mater.*, 2001, **13**, 4416–4418.
- Z. X. Yang, Y. D. Xia and R. Mokaya, *Adv. Mater.*, 2004, **16**, 727–732.
- J. C. Groen, T. Bach, U. Ziese, A. M. Paulaime-van Donk, K. P. de Jong, J. A. Moulijn and J. Pérez-Ramírez, *J. Am. Chem. Soc.*, 2005, **127**, 10792–10793.
- L. Tosheva and V. P. Valtchev, *Chem. Mater.*, 2005, **17**, 2494–2513.
- M. Choi, H. S. Cho, R. Srivastava, C. Venkatesan, D.-H. Choi and R. Ryoo, *Nat. Mater.*, 2006, **5**, 718–723.
- B. Y. Liu, Y. Z. Tan, Y. Q. Ren, C. Li, H. X. Xi and Y. Qian, *J. Mater. Chem.*, 2012, **22**, 18631–18638.
- B. Y. Liu, C. Li, Y. Q. Ren, Y. Z. Tan, H. X. Xi and Y. Qian, *Chem. Eng. J.*, 2012, **210**, 96–102.
- J. C. Groen, J. A. Moulijn and J. Pérez-Ramírez, *J. Mater. Chem.*, 2006, **16**, 2121–2131.
- J. C. Groen, W. Zhu, S. Brouwer, S. J. Huynink, F. Kapteijn, J. A. Moulijn and J. Pérez-Ramírez, *J. Am. Chem. Soc.*, 2007, **129**, 355–360.
- A. Corma, V. Fornes, J. Martínez-Triguero and S. B. Pergher, *J. Catal.*, 1999, **186**, 57–63.
- J. C. Groen, L. A. A. Peffer, J. A. Moulijn and J. Pérez-Ramírez, *Microporous Mesoporous Mater.*, 2004, **69**, 29–34.
- J. C. Groen, L. A. A. Peffer, J. A. Moulijn and J. Pérez-Ramírez, *Chem.–Eur. J.*, 2005, **11**, 4983–4994.
- S. S. Kim, J. Shah and T. J. Pinnavaia, *Chem. Mater.*, 2003, **15**, 1664–1668.
- Y. Tao, H. Kanoh and K. Kaneko, *J. Phys. Chem. B*, 2003, **107**, 10974–10976.
- W. Fan, M. A. Snyder, S. Kumar, P.-S. Lee, W. C. Yoo, A. V. McCormick, R. L. Penn, A. Stein and M. Tsapatsis, *Nat. Mater.*, 2008, **7**, 984–991.
- F.-S. Xiao, L. F. Wang, C. Y. Yin, K. F. Lin, Y. Di, J. X. Li, R. R. Xu, D. S. Su, R. Schlgl, T. Yokoi and T. Tatsumi, *Angew. Chem., Int. Ed.*, 2006, **45**, 3090–3093.
- H. Wang and T. J. Pinnavaia, *Angew. Chem., Int. Ed.*, 2006, **45**, 7603–7606.
- M. Choi, K. Na, J. Kim, Y. Sakamoto, O. Terasaki and R. Ryoo, *Nature*, 2009, **461**, 246–250.
- K. Na, C. Jo, J. Kim, K. Cho, J. Jung, Y. Seo, R. J. Messinger, B. F. Chmelka and R. Ryoo, *Science*, 2011, **333**, 328–332.
- W. Park, D. Yu, K. Na, K. E. Jelfs, B. Slater, Y. Sakamoto and R. Ryoo, *Chem. Mater.*, 2011, **23**, 5131–5137.
- K. Na, W. Park, Y. Seo and R. Ryoo, *Chem. Mater.*, 2011, **23**, 1273–1279.
- K. Cho, K. Na, J. Kim, O. Terasaki and R. Ryoo, *Chem. Mater.*, 2012, **24**, 2733–2738.
- C. Jo, J. Jung, H. S. Shin, J. Kim and R. Ryoo, *Angew. Chem., Int. Ed.*, 2013, **52**, 10014–10017.
- H. Ju, Z. P. Kai and Y. Li, *Corros. Sci.*, 2008, **50**, 865–871.
- B. Y. Liu, Z. Liu, G. C. Han and Y. H. Li, *Thin Solid Films*, 2011, **519**, 7836–7844.
- J. H. Henríquez-Román, M. Sancy, M. A. Páez, L. Padilla-Campos, J. H. Zagal, C. M. Rangel and G. E. Thompson, *J. Solid State Electrochem.*, 2005, **9**, 504–511.
- S. A. Bagshaw, E. Prouzet and T. J. Pinnavaia, *Science*, 1995, **269**, 1242–1244.
- J. C. Jansen, F. J. van der Gaag and H. van Bekkum, *Zeolites*, 1984, **4**, 369–372.
- Y. S. Tao, H. Kanoh and K. Kaneko, *J. Am. Chem. Soc.*, 2003, **125**, 6044–6045.
- Y. Xia and R. Mokaya, *J. Mater. Chem.*, 2004, **14**, 863–870.

- 41 K. S. W. Sing, D. H. Everett, R. A. W. Haul, L. Moscou, R. A. Pierotti, J. Rouquerol and T. Siemieniowska, *Pure Appl. Chem.*, 1985, **57**, 603–619.
- 42 J. A. Van Bokhoven, D. C. Koningsberger, P. Kunkeler, H. Van Bekkum and A. P. M. Kentgens, *J. Am. Chem. Soc.*, 2000, **122**, 12842–12847.
- 43 A. Lemaire, Q. Y. Wang, Y. X. Wei, Z. M. Liu and B. L. Su, *J. Colloid Interface Sci.*, 2011, **363**, 511–520.
- 44 H. Tanak, Y. Köysal, Y. Ünver, M. Yavuz, S. Işık and K. Sancak, *Struct. Chem.*, 2009, **20**, 409–416.
- 45 B. Y. Liu, Y. Q. Ren, Q. Q. Duan, F. Chen, H. X. Xi and Y. Qian, *Appl. Surf. Sci.*, 2013, **279**, 55–61.
- 46 K. F. Khaled, M. A. Amin and N. A. Al-Mobarak, *J. Appl. Electrochem.*, 2010, **40**, 601–603.
- 47 J. Jung, C. Jo, K. Cho and R. Ryoo, *J. Mater. Chem.*, 2012, **22**, 4637–4640.
- 48 V. N. Shetti, J. Kim, R. Srivastava, M. Choi and R. Ryoo, *J. Catal.*, 2008, **254**, 296–303.
- 49 B. Y. Liu, L. M. Zheng, Z. H. Zhu, C. Li, H. X. Xi and Y. Qian, *Appl. Catal., A*, 2014, **470**, 412–419.